Available online at www.sciencedirect.com
SCIENCE DIRECT®
International Journal of Thermal Sciences 44 (2005) 577–586
International Journal of Thermal Sciences
www.elsevier.com/locate/ijts

Mixed convection boundary layer flow on inclined wavy plates including the magnetic field effect ☆

Chi-Chang Wang [a,*], Cha'o-Kuang Chen [b]

[a] *Department of Information Management, Hsing Kuo University, Tainan, Taiwan 709, Republic of China*
[b] *Department of Mechanical Engineering, National Cheng Kung University, Tainan, Taiwan 701, Republic of China*

Received 4 August 2004; received in revised form 26 January 2005; accepted 3 February 2005

Abstract

A coordinate transformation and the spline alternating-direction implicit method are applied to study the mixed convection boundary layer flow along an inclined wavy plate in the presence of a transverse magnetic field. A numerical solution of the transformed boundary layer equation has been carried out for different values of magnetic field, buoyancy, wavy geometry and material parameters. Results demonstrate that the heat transfer rate and the skin-friction coefficient increase with the inclined angle. As the Prandtl number increases, the heat transfer rate and its amplitude will increase, but the skin-friction coefficient and its amplitude will decrease. The action of the magnetic field tends to accelerate the flow near the leading edge of the wavy surface and decelerate the flow far downstream of the leading edge. However, the total mixed convection heat flux along a wavy plate is higher than that of a flat plate under all circumstances.

Keywords: Mixed convection; Wavy surface; Cubic spline

1. Introduction

The laminar mixed convection along a vertical plate [1,2] or a horizontal plate [3,4] has been presented by many investigators because of its considerable practical applications. In the other hand, few studies have been carried out to examine the effect of geometric complexity, such as irregular surfaces, on the convection heat transfer. That is because complicated boundary conditions or external flow fields are difficult to deal with. However, the prediction of heat transfer from an irregular surface is of fundamental importance, and is encountered in several heat transfer devices, such as flat-plate solar collectors and flat-plate condensers in refrigerators. Irregularities frequently occur in the process of manufacture. Moreover, surfaces are sometimes intentionally roughened to enhance heat transfer because that the presence of rough surfaces disturbs the flow and alters the heat transfer rate. There now follows a discussion of research performed on some irregular surfaces.

The natural convection heat transfers from vertical wavy surfaces, such as sinusoidal surfaces, have been studied by Yao [5], Moulic and Yao [6], Rees and Pop [7], Pop and Na [8]. They solved the transformation boundary layer equations of the natural convection in Newtonian fluids by a numerical finite difference method. Results show that the local heat transfer rate varies periodically along the wavy surface, with a frequency equal to twice the frequency of the wavy surface. Later, Chiu and Chou [9] and Kim [10] performed a further study on the same geometry for micropolar fluids and non-Newtonian fluids. They found that the mean heat transfer rate and mean skin-friction coefficient are different to Newtonian fluids, but both frequencies are similar to the result of Newtonian fluids. On the other hand, these investigations into forced and mixed convection along

☆ A preliminary version of this paper was presented at CHT-04: An ICHMT International Symposium on Advances in Computational Heat Transfer, April 2004, G. de Vahl Davis and E. Leonardi (Eds.), CD-ROM Proceedings, ISBN 1-5670-174-2, Begell House, New York, 2004.

* Corresponding author. Fax: +886-6-2352973, Tel.: +886-6-2871928.
E-mail address: ccwang123@mail.hku.edu.tw (C.-C. Wang).

1290-0729/$ – see front matter
doi:10.1016/j.ijthermalsci.2005.02.001

Nomenclature

a	amplitude of wavy surface
C_f	skin-friction coefficient
C_p	specific heat of the fluid at constant pressure
g	gravitational acceleration
Gr	Grashof number
h	heat transfer coefficient
K_f	thermal conductivity
L	characteristic length
M_n	magnetic parameter
Nu_x	local Nusselt number
Nu_m	mean Nusselt number
p	pressure
Pr	Prandtl number
Re	generalized Reynolds number
Ri	Richardson number
$S(x)$	surface geometry function
U_w	x component of the velocity of the inviscid flow, evaluated at the wavy surface
T	temperature
u, v	x any y component of velocity, respectively
x, y	coordinates

Greek symbols

α	wavy amplitude-wavelength ratio
ϕ	angle of inclination from horizontal
σ	distance measured along the surface from the leading edge
θ	dimensionless temperature
μ	dynamic viscosity
ρ	density of fluid
η	coordinate
ψ	stream function

Subscripts

w	wall surface
∞	free stream condition

Superscripts

$\bar{}$	dimensional variables
$\tilde{}, \hat{}$	dimensionless quantities
$'$	derivative with respect to x

a wavy surface were carried out by Moulic and Yao [11] and Pop and Nakamura [12]. Moulic and Yao [11] proposed a simple transformation to study the mixed convection heat transfer from isothermal vertical wavy surfaces. Number results showed that the axial distribution of the local Nusselt number shows a mixture of two harmonics. The amplitude of the first harmonic is proportional to that of the wavy surface, and the natural-convection component is the second harmonic, with a frequency twice that of the wavy surface. Later, Pop and Nakamura [12] investigated the forced convection boundary layer flow of power-law fluids over wavy surfaces. They found that the skin-friction coefficient decreased with the power-law index. Furthermore, the rise and fall of the skin-friction coefficient is seen to follow changes of the surface contour.

Most of the previous studies considered only a flat plate or simple two-dimensional bodies, and few have been done on vertical wavy surfaces. Mixed convection along an inclined irregular surface imposed on a magnetic field has not been studied so far. The action of a magnetic field on the fluid has many practical applications, e.g., metals processing industry, including the control of liquid metals in continuous casting processes, plasma welding, nuclear industry and many others. Some problems of MHD mixed convection flow over a flat plate have been studied by Ibrahim and Hady [13] and Mohammadein and Gorla [14]. In this study a simple coordinate transformation is employed to transform a complex wavy surface to a flat plate, and the obtained boundary layer equations are then solved by the spline alternating-direction implicit method. The effects of the magnetic field parameter, the amplitude-wavelength ratio, the angle of inclination from horizontal, the Richardson number, the parameter $Ri/Re^{1/2}$ and the Prandtl number on the skin-friction coefficient and the Nusselt number have been examined in detail.

2. Mathematical formulation

Consider a stagnant, semi-infinite symmetric body with a wavy surface and a cusped leading edge as shown in Fig. 1. The axis of symmetry is aligned with the oncoming uniform stream. The wavy surface is described by $\bar{S}(\bar{x}) = \bar{a}\sin^2(\pi\bar{x}/L)$, where $\bar{a}$ is the amplitude of the wavy surface. The temperature of the wavy surface is held at a constant value T_w, which is higher than the ambient temperature T_∞. The electrically conducting fluids are assumed to be Newtonian fluids with constant fluid properties, except for the density in the buoyancy force term (i.e., Boussinesq approximation). Moreover, the flow is considered to be laminar, incompressible, steady and two-dimensional. Viscous dissipation is neglected for it has negligible effect. A magnetic field with a constant magnetic flux density, B_0, is applied. In magneto fluid mechanics, fluid motion is governed by the laws of conservation of mass, momentum and energy. The equations of continuity and energy remain unchanged. The momentum is modified from Maxwell's field equation and Ohm's law. Since the above assumptions are designed to keep the theoretical model as simple as possible, the governing equations may be written in the following form

$$\frac{\partial\bar{u}}{\partial\bar{x}} + \frac{\partial\bar{v}}{\partial\bar{y}} = 0 \tag{1}$$

$$\rho\left(\bar{u}\frac{\partial\bar{u}}{\partial\bar{x}}+\bar{v}\frac{\partial\bar{u}}{\partial\bar{y}}\right)$$
$$=-\frac{\partial\bar{p}}{\partial\bar{x}}+\mu\left(\frac{\partial^2\bar{u}}{\partial\bar{x}^2}+\frac{\partial^2\bar{u}}{\partial\bar{y}^2}\right)$$
$$+\rho g\beta\left((T-T_\infty)\sin\phi+\frac{\partial}{\partial\bar{x}}\int_{\bar{y}}^{\infty}(T-T_\infty)\cos\phi\,\mathrm{d}\bar{y}\right)$$
$$-\sigma B_0^2\bar{u} \tag{2}$$

$$\rho\left(\bar{u}\frac{\partial\bar{v}}{\partial\bar{x}}+\bar{v}\frac{\partial\bar{v}}{\partial\bar{y}}\right)$$
$$=-\frac{\partial\bar{p}}{\partial\bar{y}}+\mu\left(\frac{\partial^2\bar{v}}{\partial\bar{x}^2}+\frac{\partial^2\bar{v}}{\partial\bar{y}^2}\right)+\rho g\beta(T-T_\infty)\cos\phi \tag{3}$$

$$\rho C_p\left(\bar{u}\frac{\partial T}{\partial\bar{x}}+\bar{v}\frac{\partial T}{\partial\bar{y}}\right)=K_f\left(\frac{\partial^2T}{\partial\bar{x}^2}+\frac{\partial^2T}{\partial\bar{y}^2}\right) \tag{4}$$

The boundary conditions are

(a) On the wavy surface, $\bar{y}=\overline{S}(\bar{x})$

$$T=T_w,\qquad \bar{u}=\bar{v}=0 \tag{5}$$

(b) Matching with the free stream, $\bar{y}\to\infty$

$$T\to T_\infty,\qquad \bar{u}\to\overline{U}_w(\bar{x}),\qquad \bar{p}\to\bar{p}_\infty(\bar{x}) \tag{6}$$

Here $\bar{u}$ and $\bar{v}$ are the components of the velocity along the $\bar{x}$ and $\bar{y}$ directions. T and $\bar{p}$ are the temperature and the pressure. ρ, μ and β are the density, viscosity and thermal expansion coefficient of the fluid. K_f and C_p are the thermal conductivity and the specific heat of the fluid at constant pressure. $\overline{U}_w(\bar{x})$ is the $\bar{x}$ component of the inviscid velocity at the free surface $\bar{y}=\overline{S}(\bar{x})$.

The dimensionless variables are defined as

$$\tilde{x}=\frac{\bar{x}}{L},\qquad \tilde{y}=\frac{\bar{y}}{L},\qquad \alpha=\frac{\bar{a}}{L},\qquad S(\tilde{x})=\frac{\overline{S}(\bar{x})}{L}$$
$$\tilde{u}=\frac{\bar{u}}{U_\infty},\qquad \tilde{v}=\frac{\bar{v}}{U_\infty},\qquad \theta=\frac{T-T_\infty}{T_w-T_\infty}$$
$$U_w=\frac{\overline{U}_w}{U_\infty},\qquad \tilde{p}=\frac{\bar{p}}{\rho U_\infty^2}$$
$$Re=\frac{\rho U_\infty L}{\mu},\qquad Gr=\frac{g\beta(T_w-T_\infty)\rho^2L^3}{\mu^2},\qquad Ri=\frac{Gr}{Re^2}$$
$$Pr=\frac{\mu C_p}{K_f},\qquad M_n=\frac{\sigma LB_0^2}{\rho U_\infty} \tag{7}$$

Here U_∞ is the free stream velocity. Substituting (7) into Eqs. (1)–(4) gives

$$\frac{\partial\tilde{u}}{\partial\tilde{x}}+\frac{\partial\tilde{v}}{\partial\tilde{y}}=0 \tag{8}$$
$$\tilde{u}\frac{\partial\tilde{u}}{\partial\tilde{x}}+\tilde{v}\frac{\partial\tilde{u}}{\partial\tilde{y}}$$
$$=-\frac{\partial\tilde{p}}{\partial\tilde{x}}+\frac{1}{Re}\left(\frac{\partial^2\tilde{u}}{\partial\tilde{x}^2}+\frac{\partial^2\tilde{u}}{\partial\tilde{y}^2}\right)$$
$$+Ri\left(\theta\sin\phi+\frac{\partial}{\partial\tilde{x}}\int_{\tilde{y}}^{\infty}\theta\cos\phi\,\mathrm{d}\tilde{y}\right)-M_n\tilde{u} \tag{9}$$

$$\tilde{u}\frac{\partial\tilde{v}}{\partial\tilde{x}}+\tilde{v}\frac{\partial\tilde{v}}{\partial\tilde{y}}=-\frac{\partial\tilde{p}}{\partial\tilde{y}}+\frac{1}{Re}\left(\frac{\partial^2\tilde{u}}{\partial\tilde{x}^2}+\frac{\partial^2\tilde{u}}{\partial\tilde{y}^2}\right)+Ri\,\theta\sin\phi \tag{10}$$

$$\tilde{u}\frac{\partial\theta}{\partial\tilde{x}}+\tilde{v}\frac{\partial\theta}{\partial\tilde{y}}=\frac{1}{RePr}\left(\frac{\partial^2\theta}{\partial\tilde{x}^2}+\frac{\partial^2\theta}{\partial\tilde{y}^2}\right) \tag{11}$$

The first step is to transform the irregular wavy surface into a flat surface by using Prandtl's transposition theorem [15]. The theorem means that the flow is displaced by the amount of the vertical displacement of an irregular solid surface, and the vertical component of the velocity is adjusted according to the slope of the surface. The form of the boundary layer equation is invariant under this transformation, and the surface conditions can be applied to the transformed flat surface. This allows the boundary conditions to be easily incorporated into any numerical method. In order to transform the above governing equations, the following dimensionless quantities are defined.

$$\hat{x}=\tilde{x},\qquad \hat{y}=\big(\tilde{y}-S(\tilde{x})\big)Re^{1/2}$$
$$\hat{u}=\tilde{u},\qquad \hat{v}=\big(\tilde{v}-S'\tilde{u}\big)Re^{1/2},\qquad \hat{p}=\tilde{p}-\tilde{p}_\infty \tag{12}$$

Therefore, by substituting Eq. (12) into Eqs. (8)–(11) and letting $Re\to\infty$ (boundary layer approximation), the governing equations are transformed from an irregular wavy surface into a flat surface. The transformed boundary layer equations are given as

$$\frac{\partial\hat{u}}{\partial\hat{x}}+\frac{\partial\hat{v}}{\partial\hat{y}}=0 \tag{13}$$
$$\hat{u}\frac{\partial\hat{u}}{\partial\hat{x}}+\hat{v}\frac{\partial\hat{u}}{\partial\hat{y}}$$
$$=-\frac{\partial\hat{p}}{\partial\hat{x}}+Re^{1/2}S'\frac{\partial\hat{p}}{\partial\hat{y}}+\big(1+S'^2\big)\frac{\partial^2\hat{u}}{\partial\hat{y}^2}$$
$$+Ri\big(\sin\phi+S'\cos\phi\big)\theta$$
$$+\frac{Ri}{\sqrt{Re}}\int_{\hat{y}}^{\infty}\frac{\partial\theta}{\partial\hat{x}}\cos\phi\,\mathrm{d}\hat{y}-M_n\hat{u} \tag{14}$$

$$\hat{u}^2S''=S'\frac{\partial\hat{p}}{\partial\hat{x}}-Re^{1/2}\big(1+S'^2\big)\frac{\partial\hat{p}}{\partial\hat{y}}$$
$$+Ri\big(\cos\phi-S'\sin\phi-S'^2\cos\phi\big)\theta$$
$$-\frac{Ri}{\sqrt{Re}}\int_{\hat{y}}^{\infty}\frac{\partial\theta}{\partial\hat{x}}\cos\phi\,\mathrm{d}\hat{y}-M_n\hat{u} \tag{15}$$

$$\hat{u}\frac{\partial\theta}{\partial\hat{x}}+\hat{v}\frac{\partial\theta}{\partial\hat{y}}=\frac{1}{Pr}\big(1+S'^2\big)\frac{\partial^2\theta}{\partial\hat{y}^2} \tag{16}$$

Eq. (15) indicates that the pressure gradient along y-direction is $O(Re^{-1/2})$. Therefore, from the inviscid flow solution, we can express the pressure gradient along x-direction as

$$\frac{\partial\hat{p}}{\partial\hat{x}}=-\big(1+S'^2\big)U_wU_w'+S'S''U_w^2+M_nU_w \tag{17}$$

The transformed momentum Eqs. (14) and (15) can be combined into one equation by eliminating the pressure gradient $\partial\hat{p}/\partial\hat{y}$, and so, we have

$$\hat{u}\frac{\partial\hat{u}}{\partial\hat{x}}+\hat{v}\frac{\partial\hat{u}}{\partial\hat{y}}=\frac{1}{1+S'^2}\left(-\frac{\partial\hat{p}}{\partial\hat{x}}+Ri\big(\sin\phi+2S'^2\cos\phi\big)\theta+\frac{Ri}{\sqrt{Re}}\int_{\hat{y}}^{\infty}\frac{\partial\theta}{\partial\hat{x}}\cos\phi\,\mathrm{d}\hat{y}-S'S''\hat{u}^2-M_n\hat{u}\right)+\big(1+S'^2\big)\frac{\partial^2\hat{u}}{\partial\hat{y}^2} \tag{18}$$

In order to remove the singularity at $x=0$, Eqs. (13), (16) and (18) are further transformed by means of the following variables

$$x=\hat{x},\qquad y=\hat{y}\left(\frac{2\hat{x}}{U_w}\right)^{-1/2} \tag{19}$$

$$u=\frac{\hat{u}}{U_w},\qquad v=\hat{v}\left(\frac{2\hat{x}}{U_w}\right)^{1/2} \tag{20}$$

Then Eqs. (13), (16) and (18) are transforms into

$$2x\frac{\partial u}{\partial x}-y\left(1-x\frac{U_w'}{U_w}\right)\frac{\partial u}{\partial y}+\frac{\partial v}{\partial y}+2x\frac{U_w'}{U_w}u=0 \tag{21}$$

$$\begin{aligned}&2xu\frac{\partial u}{\partial x}+\left[v-yu\left(1-x\frac{U_w'}{U_w}\right)\right]\frac{\partial u}{\partial y}+2x\big(u^2-1\big)\left(\frac{S'S''}{1+S'^2}+\frac{U_w'}{U_w}\right)\\&=\frac{2x}{U_w^2(1+S'^2)}Ri\big(\sin\phi+2S'^2\cos\phi\big)\theta+\frac{2x^{1/2}}{U_w^{5/2}(1+S'^2)}\frac{Ri}{\sqrt{Re}}\cos\phi\left[\left(1-x\frac{U_w'}{U_w}\right)\times\left(\int_y^{\infty}\theta\,\mathrm{d}y+y\theta\right)+2x\int_y^{\infty}\frac{\partial\theta}{\partial x}\mathrm{d}y\right]\\&\quad+\big(1+S'^2\big)\frac{\partial^2u}{\partial y^2}+\frac{2x}{U_w(1+S'^2)}M_n(1-u)\end{aligned} \tag{22}$$

$$2xu\frac{\partial\theta}{\partial x}+\left[v-yu\left(1-x\frac{U_w'}{U_w}\right)\right]\frac{\partial\theta}{\partial y}=\frac{1+S'^2}{Pr}\frac{\partial^2\theta}{\partial y^2} \tag{23}$$

The corresponding boundary conditions are

$$\begin{aligned}&y=0:\quad \theta=1,\qquad u=v=0\\&y\to\infty:\quad \theta\to0,\qquad u\to1\end{aligned} \tag{24}$$

The last step is to obtain the surface velocity $U_w(x)$. Moulic and Yao [11], Pop and Nakamura [12] and Cheng and Wang [16] have obtained good results for smaller values of the amplitude-wavelength ratio ($\alpha\ll1$) by expressing the stream function as a two-term series. The series solution in Cheng and Wang [16] can be expanded as

$$U_w(x)=1+\alpha\left[-\pi\cos(2\pi x)+\int_0^{\infty}\frac{\sin(2\pi t)}{x+t}\mathrm{d}t\right]+\mathrm{O}\big(\alpha^2\big) \tag{25}$$

In this present study, for larger amplitude-wavelength ratio, the numerical method (SOR) and the transformed coordinates have been used to solve the potential flow and to determine the surface velocity U_w. Therefore, the streamline equation and the transformed coordinates can be written as following

$$\frac{\partial^2\psi}{\partial\tilde{x}^2}+\frac{\partial^2\psi}{\partial\tilde{y}^2}=0 \tag{26}$$

$$x=\tilde{x},\qquad \eta=\tilde{y}-\tilde{S}(\tilde{x}) \tag{27}$$

Thus, we can get the transformed equation and the velocity $U_w(x)$

$$\frac{\partial^2\psi}{\partial x^2}-S''\frac{\partial\psi}{\partial\eta}-2S'\frac{\partial^2\psi}{\partial x\,\partial\eta}+\big(1+S'^2\big)\frac{\partial^2\psi}{\partial\eta^2}=0 \tag{28}$$

$$U_w=\frac{\partial\psi}{\partial\eta}\Big|_{\eta=0} \tag{29}$$

Since the flow and the temperature fields are obtained, several important quantities can be calculated as follows.

The local Nusselt number is defined as

$$Nu_{\bar{x}}=\frac{h_{\bar{x}}\bar{x}}{K_f}=\frac{-\frac{\partial T}{\partial n}\bar{x}}{T_w-T_\infty} \tag{30}$$

$$\frac{\partial T}{\partial n}=\sqrt{\left(\frac{\partial T}{\partial\bar{x}}\right)^2+\left(\frac{\partial T}{\partial\bar{y}}\right)^2} \tag{31}$$

where $\partial/\partial n$ represents differentiation along the normal to the surface. As $Gr/Re^2\neq0$ the local Nusselt number can be expressed as

$$\left(\frac{4}{Gr_{\bar{x}}}\right)^{1/4}Nu_{\bar{x}}=-\left(\frac{Gr}{Re^2}x\right)^{-1/4}U_w^{1/2}\big(1+S'^2\big)^{1/2}\frac{\partial\theta}{\partial y}\Big|_{y=0} \tag{32}$$

The total Nusselt number is obtained by averaging the heat transfer flux over the surface from the leading edge to $S(x)$.

$$Nu_m=\frac{h_m\bar{\sigma}(\bar{x})}{K_f} \tag{33}$$

where

$$h_m=\frac{q_m}{T_w-T_\infty} \tag{34}$$

$$q_m=\frac{1}{\sigma}\int_0^{\sigma}-K_f\frac{\partial T}{\partial n}\,\mathrm{d}\sigma \tag{35}$$

$$\sigma=\int_0^{x}\big(1+S'^2\big)^{1/2}\,\mathrm{d}x \tag{36}$$

Then the quantity of $(4/Gr_{\bar{x}})^{1/4}Nu_m$ can be expressed as

$$\left(\frac{4}{Gr_{\bar{x}}}\right)^{1/4} Nu_m = -\left(\frac{Gr}{Re^2}x\right)^{-1/4}\left(\frac{2}{x}\right)^{1/2}\int_0^x \left(\frac{U_w}{2x}\right)^{1/2} \times \left(1+S'^2\right)\frac{\partial\theta}{\partial y}\Big|_{y=0}\mathrm{d}x \tag{37}$$

The shear force at the surface and the skin-friction coefficient C_f are defined as

$$\tau_w = \mu\left(\frac{\partial\bar{u}}{\partial\bar{y}} - \frac{\partial\bar{v}}{\partial\bar{x}}\right)_{\bar{y}=\overline{S}(\bar{x})} \tag{38}$$

$$C_f = \frac{2\tau_w}{\rho U_\infty^2} \tag{39}$$

Substituting Eq. (38) into Eq. (39) and ignoring the small order terms yield the following equation

$$Ri^{-1}\left(\frac{Gr}{4x}\right)^{1/4} C_f = \left(\frac{Gr}{Re^2}x\right)^{-3/4} U_w^{3/2}\left(1+S'^2\right)\frac{\partial u}{\partial y}\Big|_{y=0} \tag{40}$$

3. Numerical method

The governing differential Eqs. (21)–(23), combined with the appropriate boundary conditions (24), have been solved by using the spline alternating-direction implicit method [17], an improved version of the cubic spline collocation method [18]. Using the false transient technique, we can write Eqs. (21)–(23) in the following form

$$\varphi_{i,j}^{n+1} = F_{i,j} + G_{i,j}m_{i,j}^{n+1} + S_{i,j}M_{i,j}^{n+1} \tag{41}$$

where i and j refer to the computational nodes, n is the time step, φ represents u or θ, and m and M are the first and the second derivatives of φ with respect to y, respectively. $F_{i,j}$, $G_{i,j}$ and $S_{i,j}$ are the known coefficients evaluated at the previous time step, as shown in the following.

As φ represents u

$$\begin{aligned} F_{i,j}\colon\ & u_{i,j}^n + \Delta\tau\Bigg[-2xu_{i,j}^{n+1}\left(\frac{\partial u}{\partial x}\right)_{i,j}^{n+1} \\ & - 2x\left(\left(u_{i,j}^{n+1}\right)^2 - 1\right)\left(\frac{S'S''}{1+S'^2} + \frac{U_w'}{U_w}\right) \\ & + \frac{2x}{U_w^2(1+S'^2)}Ri\left(\sin\phi + 2S'^2\cos\phi\right)\theta_{i,j}^{n+1} \\ & + \frac{2x}{U_w(1+S'^2)}M_n\left(1-u_{i,j}^{n+1}\right) + \frac{2x^{1/2}}{U_w^{5/2}(1+S'^2)} \\ & \times \frac{Ri}{\sqrt{Re}}\cos\phi\Bigg[\left(1-x\frac{U_w'}{U_w}\right)\left(\int_y^\infty \theta_{i,j}^{n+1}\,\mathrm{d}y + y\theta_{i,j}^{n+1}\right) \\ & + 2x\int_y^\infty\left(\frac{\partial\theta}{\partial x}\right)_{i,j}^{n+1}\mathrm{d}y\Bigg]\Bigg] \end{aligned} \tag{42}$$

$$G_{i,j}\colon\ -\Delta\tau\left[v_{i,j}^{n+1} - yu_{i,j}^{n+1}\left(1-x\frac{U_w'}{U_w}\right)\right] \tag{43}$$

$$S_{i,j}\colon\ \Delta\tau\left(1+S'^2\right) \tag{44}$$

As φ represents θ

$$F_{i,j}\colon\ \theta_{i,j}^n + \Delta\tau\left[-2xu_{i,j}^{n+1}\left(\frac{\partial\theta}{\partial x}\right)_{i,j}^{n+1}\right] \tag{45}$$

$$G_{i,j}\colon\ -\Delta\tau\left[v_{i,j}^{n+1} - yu_{i,j}^{n+1}\left(1-x\frac{U_w'}{U_w}\right)\right] \tag{46}$$

$$S_{i,j}\colon\ \frac{\Delta\tau}{Pr}\left(1+S'^2\right) \tag{47}$$

by using cubic spline collocation relations described in [18], Eq. (41) may be written in tridiagonal form as

$$A_{i,j}\Omega_{i,j}^{n+1} + B_{i,j}\Omega_{i,j}^{n+1} + C_{i,j}\Omega_{i,j}^{n+1} = D_{i,j} \tag{48}$$

where Ω represents u or θ, or its first and second derivatives. The Thomas algorithm is then employed to solve Eq. (48).

Since the singularity at $x = 0$ has been removed by the scaling, the computation starts from $x = 0$, and then marches downstream. At every x-station, the iteration process continues until the convergence criterion is achieved

$$\left|\frac{\Omega_{i,j}^{n+1} - \Omega_{i,j}^n}{\Omega_{i,j}^{n+1}}\right| \leqslant 1\times 10^{-5} \tag{49}$$

Table 1
The local heat transfer rate $(2/Re_{\bar{x}})^{1/2}Nu_{\bar{x}}$ and the local skin-friction coefficient $(2Re_{\bar{x}})^{1/2}C_f$: (a) for different grids; (b) for different Prandtl numbers

	$(2/Re_{\bar{x}})^{1/2}Nu_{\bar{x}}$		$(2Re_{\bar{x}})^{1/2}C_f$	
(a) Present solutions for $Ri = 100$, $Ri/Re^{1/2} = 10$, $Pr = 6.93$, $\alpha = 0.2$, $M_n = 1$, $\phi = 60°$, $x \in [0, 4]$, $y \in [0, 7]$				
	$x = 0.2$	$x = 4$	$x = 0.2$	$x = 4$
300×20	2.44110	4.02601	22.48473	124.19864
300×50	2.43961	3.96990	22.32297	119.75632
300×100	2.43968	3.98526	22.30522	119.57684
200×50	2.43952	3.97021	22.28112	118.95212
100×50	2.45129	3.99603	22.25373	117.62628
50×50	2.48732	3.99409	21.96970	104.52509
200×50[a]	2.44075	4.14664	22.33547	120.71258
200×50[b]	2.44182	3.96830	25.87353	119.71943
(b) Present solutions for $Gr/Re^{5/2} = 5$, $\alpha = M_n = \phi = 0$, grid size is 200×50[c]				
	$x = 0.36$	$x = 4$	$x = 0.36$	$x = 4$
$Pr = 0.70$	0.67795 (0.67627)	0.83401 (0.83056)	5.86468 (5.83583)	11.57735 (11.43165)
$Pr = 7.00$	2.88922 (2.87849)	5.30618 (5.28436)	1.25847 (1.25907)	1.51646 (1.51674)

[a] Uniform grid (y direction).
[b] Uniform grid (x direction).
[c] The values in parenthesis are obtained by Ramachandram et al. [3].

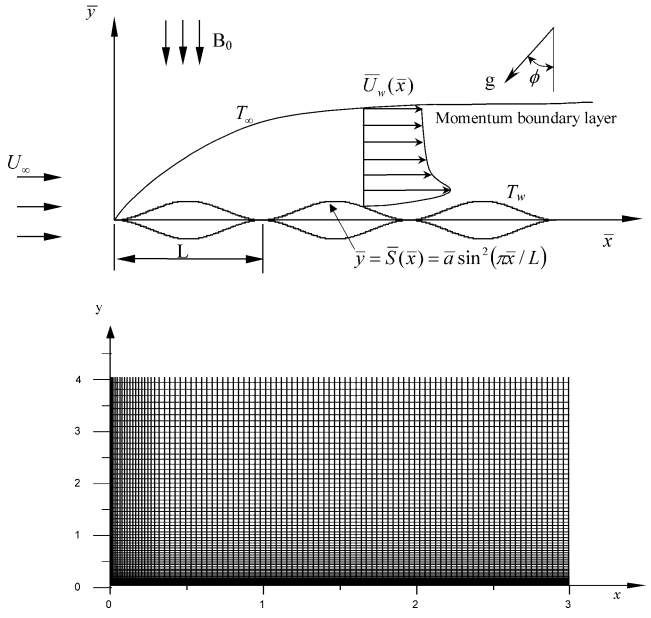

Fig. 1. Physical model and grid system.

4. Results and discussion

Since the spline alternating-direction implicit method can evaluate the spatial derivative terms directly without any finite difference discretization, the gradient boundary conditions may be represented more accurately and the irregular boundaries are easier to deal with. An accuracy test of grid fineness is made for the grids of 300×20, 300×50, 300×100, 200×50, 100×50, 50×50. Results are shown in Table 1(a). The differences between the results for grids of 200×50 and of 300×100 are less than 0.2% in the local Nusselt number and in the skin-friction coefficient at $Ri = 100$, $Ri/Re^{1/2} = 10$, $Pr = 6.93$, $\alpha = 0.2$, $M_n = 1$, $\phi = 60°$, $x \in [0, 4]$, $y \in [0, 7]$. Therefore, as shown in Fig. 1, the present work employs 200×50 nonuniform grids with smaller spacing mesh points near the fluid-solid boundary at y direction and near the leading edge at x direction. In order to verify the accuracy of the solution, numerical results are obtained for the mixed convection over the horizontal flat plate (i.e., $\alpha = 0$) for $Pr = 0.7$ and $Pr = 7.0$. As shown in Table 1(b), the skin-friction coefficient and the local Nusselt number calculated are found to be in good agreement with results obtained from Ramachandram et al. [3].

In order to determine the surface velocity U_w in Eqs. (21)–(23), the stream function in Eq. (28) is calculated by using the SOR method. The streamline for $\alpha = 0.2$ and the axial distributions of the inviscid surface velocity $U_w(x)$ are shown in Figs. 2 and 3, respectively. By comparing the results of numerical method and Eq. (25), it will be observed that the two inviscid surface velocities $U_w(x)$ match closely for $\alpha = 0.1$ but have some obvious discrepancies for $\alpha = 0.2$. This is because that the inviscid velocity obtained in Eq. (25) is valid only for small values of the amplitude-wavelength ratio. However, the inviscid surface velocity

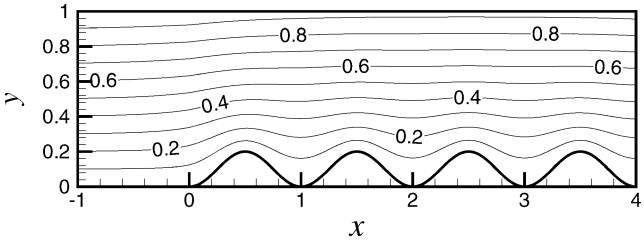

Fig. 2. Streamlines of flow for $\alpha = 0.2$.

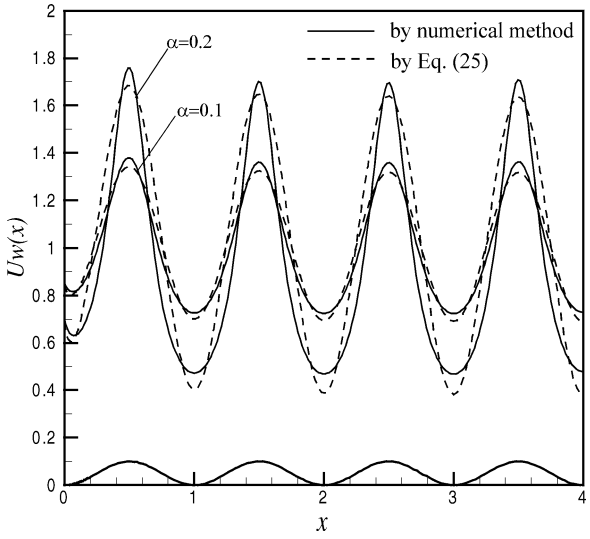

Fig. 3. Inviscid surface velocity distribution.

shows a variation periodically along the wavy surface with a cycle equals to that of the surface. The flow accelerates along the portion of the surface from trough to crest, where the slope S' is positive; while it decelerates along the portion of the surface from crest to trough, where the slope S' is negative. Moreover, the amplitude of inviscid surface velocity tends to increase as the amplitude-wavelength ratio increases.

(a) The influence of the inclined angle and the Prandtl number

Figs. 4–6 show the axial distribution of the local skin-fiction coefficient $Ri^{-1}(Gr/4x)^{1/4}C_f$, the local Nusselt number $(4/Gr_{\bar{x}})^{1/4}Nu_{\bar{x}}$ and the average Nusselt number $(4/Gr_{\bar{x}})^{1/4}Nu_m$ for $\alpha = 0.2$, $Ri = 500$, $Ri/Re^{1/2} = 10$ and $M_n = 0$, including results for the limiting case of a flat plate ($\alpha \to 0$) for comparison. As shown in Fig. 4, the curves for vertical wavy plate show the presence of two harmonics, which have a frequency twice that of the wavy surface. The first harmonic is due to the pressure gradient parameter, which involves U_w and its derivative; the second harmonic is due to the centrifugal, buoyancy, and diffusion terms, which involve S'^2 and $S'S''$. As the inclined angle decreases, the second harmonic becomes inconspicuous. This may be explained as follows. Though the effect of the buoyancy term $Ri/Re^{1/2}$ increases as $\cos\phi$ when the wavy plate is inclined

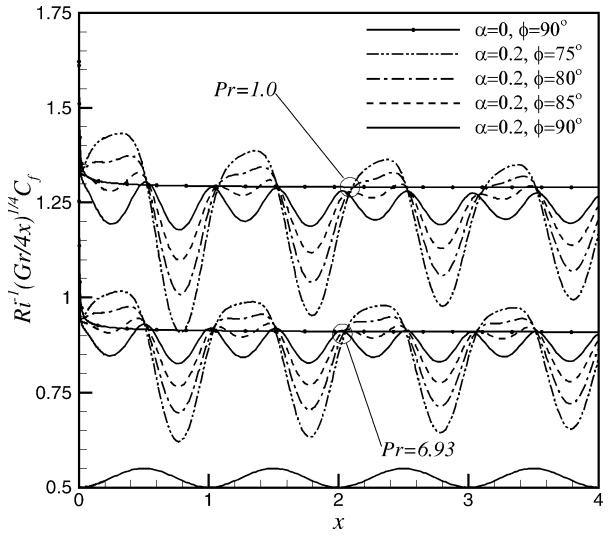

Fig. 4. Axial distribution of $Ri^{-1}(Gr/4x)^{1/4}C_f$ for different inclined angles and Prandtl numbers at $\alpha = 0.2$, $Ri = 500$, $Ri/Re^{1/2} = 10$ and $M_n = 0$.

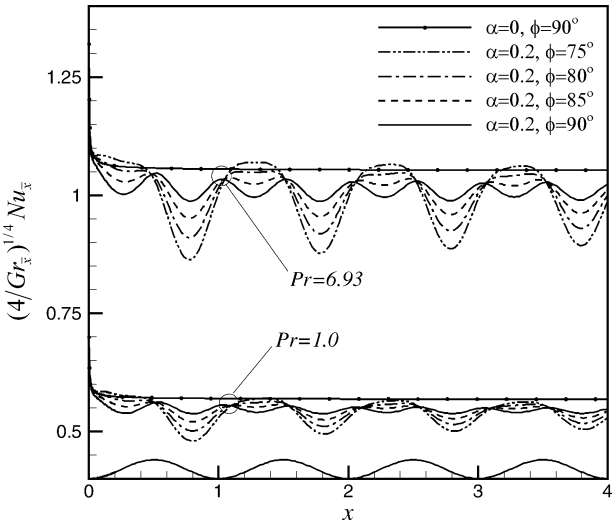

Fig. 5. Axial distribution of $(4/Gr_{\bar{x}})^{1/4}Nu_{\bar{x}}$ for different inclined angles and Prandtl numbers at $\alpha = 0.2$, $Ri = 500$, $Ri/Re^{1/2} = 10$ and $M_n = 0$.

from the horizontal, the effect of the Richardson number (i.e., Ri) decreases as $\sin\phi$ in Eq. (22). It should note that the buoyancy term Ri is larger than the buoyancy term $Ri/Re^{1/2}$ for a boundary layer flow. Therefore, as ϕ decreases, the total buoyancy force effect diminishes and the second harmonic cannot be found clearly.

In previous study, the quantity $(4/Gr_{\bar{x}})^{1/4}Nu_{\bar{x}}$ is a constant for free convection along a flat plate. In case of mixed convection boundary layer flow along a flat plate, as shown in Fig. 5, forced convection is the dominant mode of heat transfer near the leading edge, while further downstream, free convection becomes the dominant mode of heat transfer. Hence, the curve of $(4/Gr_{\bar{x}})^{1/4}Nu_{\bar{x}}$ versus x for the flat plate approaches a constant value far downstream of the leading edge. In the other hand, the curves for wavy surfaces exhibit the same periodic behavior as in Fig. 4. However, the mean

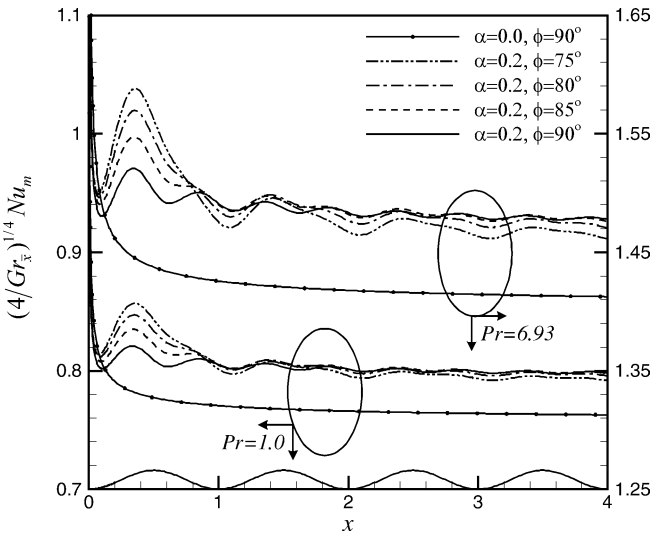

Fig. 6. Axial distribution of $(4/Gr_{\bar{x}})^{1/4}Nu_m$ for different inclined angles and Prandtl numbers at $\alpha = 0.2$, $Ri = 500$, $Ri/Re^{1/2} = 10$ and $M_n = 0$.

variation of $(4/Gr_{\bar{x}})^{1/4}Nu_{\bar{x}}$ with x is nearly constant, except near the leading edge.

As shown in Eq. (37), the average Nusselt number may be obtained by averaging the heat flux over the wavy surface from the leading edge of the wavy surface to $\sigma(x)$. Besides, the heat transfer area is based on the total area of each wave and not on projected area. From the standpoint of the average Nusselt number as shown in Fig. 6, it appears that the highest average Nusselt numbers belong to the first wave and the average Nusselt numbers stay uniform downstream of the third wave. The values of $(4/Gr_{\bar{x}})^{1/4}Nu_m$ for wavy plate show the same periodic behavior as the local Nusselt numbers and are uniformly larger than that of the corresponding flat plate, except near the leading edge of the wavy plate. This outcome is due to that although the $(4/Gr_{\bar{x}})^{1/4}Nu_{\bar{x}}$ of the wavy plate is almost everywhere smaller than that of the flat plate in Fig. 5, the wavy plate has larger heat transfer area to raise the average heat transfer rate. In addition, an increase in angle of inclination tends to increase the mean heat transfer rate. For the vertical plate, the buoyancy force is everywhere parallel to the surface. The component of the buoyancy force tangential to the inclined surface is less than the whole buoyancy force. Hence, the mean heat transfer rate for an inclined wavy plate is less than that for a vertical plate with equal wavy amplitude-wavelength ratio.

In Figs. 4–6, it is also seen that for the given values of α, ϕ, Ri, $Ri/Re^{1/2}$ and M_n, a higher Prandtl number results in a smaller skin-friction coefficient. This outcome is due to that the lower density exhibits a greater sensitivity to the buoyancy force effect, thus causes a larger change in the velocity gradients at the wall (see Fig. 7) and increases the skin-friction coefficient. On the other hand, the local and average Nusselt numbers for $Pr = 6.93$ are larger than that for $Pr = 1.0$. This is because as the Prandtl number increases, the thermal boundary layer thickness decreases and the surface temperature gradient increases (see Fig. 8) which results

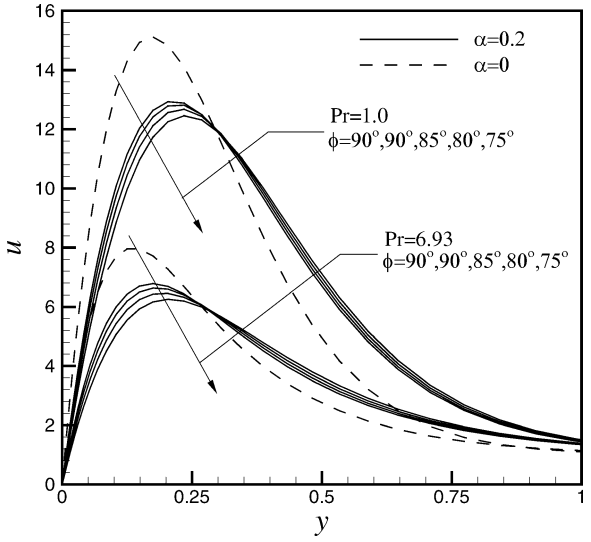

Fig. 7. Axial velocity profiles for different inclined angles and Prandtl numbers at $x = 1.75$, $\alpha = 0.2$, $Ri = 500$, $Ri/Re^{1/2} = 10$ and $M_n = 0$.

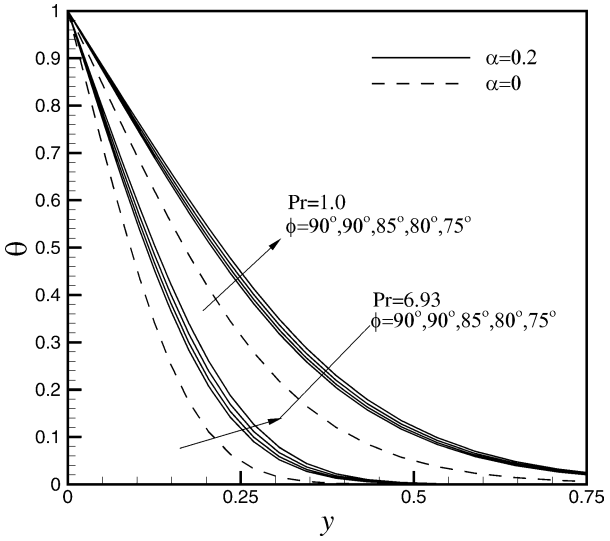

Fig. 8. Temperature distribution for different inclined angles and Prandtl numbers at $x = 1.75$, $\alpha = 0.2$, $Ri = 500$, $Ri/Re^{1/2} = 10$ and $M_n = 0$.

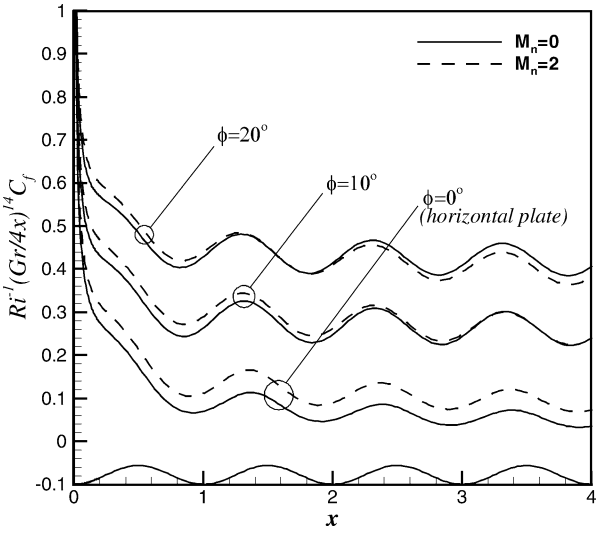

Fig. 9. Axial distribution of $Ri^{-1}(Gr/4x)^{1/4}C_f$ for different magnetic field strengths at $\alpha = 0.01$, $Ri = 50$, $Ri/Re^{1/2} = 5$ and $Pr = 6.9$.

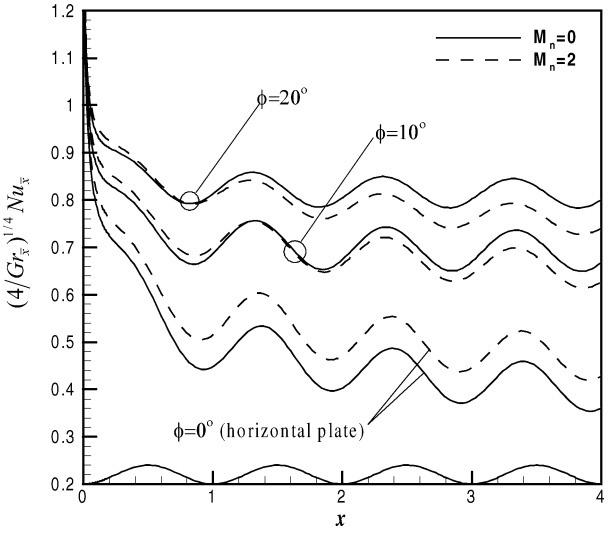

Fig. 10. Axial distribution of $(4/Gr_{\bar{x}})^{1/4}Nu_{\bar{x}}$ for different magnetic field strengths at $\alpha = 0.01$, $Ri = 50$, $Ri/Re^{1/2} = 5$ and $Pr = 6.9$.

in a higher rate of heat transfer from the surface. Furthermore, an increase in Prandtl number for the wavy plate tends to increase the amplitudes of the local and the average Nusselt numbers but slightly decreases that of the skin-friction coefficient.

(b) The influence of the magnetic field strength

Figs. 9–11 show variations of the skin-friction coefficient, the local and the average Nusselt numbers along the wavy surface for smaller inclined angle when $\alpha = 0.01$, $Ri = 50$, $Ri/Re^{1/2} = 5$ and $Pr = 6.9$. It is seen that the influence of buoyancy increases when the inclined angle increases from horizontal, thereby causing increases in the skin-friction coefficient and the Nusselt number. Moreover, the inclined angle tends to increase the amplitude of the skin-friction coefficient but decrease that of the Nusselt number. When the wavy plate imposed on a magnetic field, the skin-friction coefficient and the Nusselt number increase everywhere for the horizontal plate (i.e., $\phi = 0$). It should be noted that as ϕ increases to 10 or 20, the skin-friction coefficient and the Nusselt number also increase near the leading edge of the plate but decrease further downstream. This result may be expanded in Eqs. (17) and (22), the magnetic parameter (i.e., M_n) causes a thrust when axial velocity $u < 1$ and causes a resistance when axial velocity $u > 1$. Thereby, the skin-friction coefficient and the Nusselt number increase for a small inclined angle or near the leading edge (where the axial velocity $u \leqslant 1$), since here the forced convection is the dominant mode of heat transfer. On the other hand, for a larger inclined angle or far downstream of the leading edge (where the maximum axial velocity $u_{\max} \gg 1$), because of

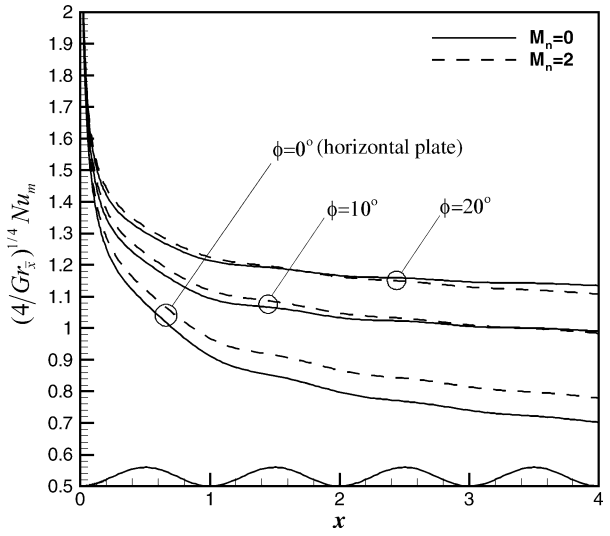

Fig. 11. Axial distribution of $(4/Gr_{\bar{x}})^{1/4}Nu_m$ for different magnetic field strengths at $\alpha = 0.01$, $Gr/Re^2 = 50$, $Gr/Re^{5/2} = 5$ and $Pr = 6.9$.

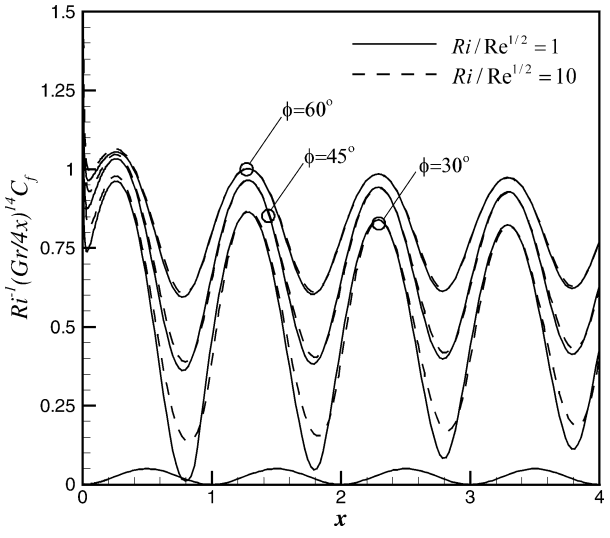

Fig. 12. Axial distribution of $Ri^{-1}(Gr/4x)^{1/4}C_f$ for different values of $Ri/Re^{1/2}$ at $\alpha = 0.1$, $Ri = 100$, $M_n = 0$ and $Pr = 6.93$.

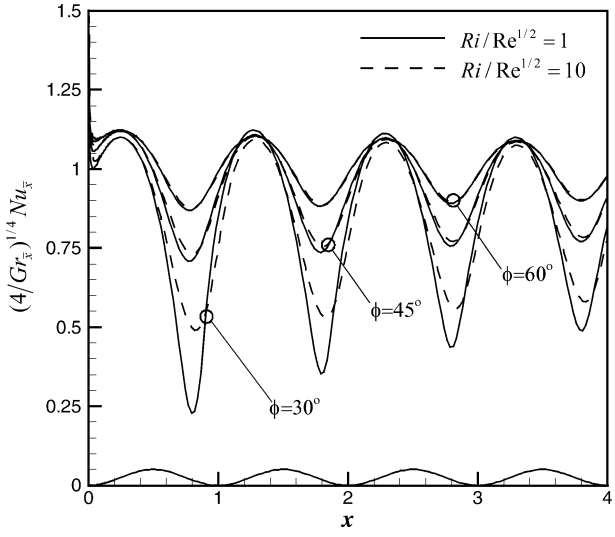

Fig. 13. Axial distribution of $(4/Gr_{\bar{x}})^{1/4}Nu_x$ for different values of $Ri/Re^{1/2}$ at $\alpha = 0.1$, $Ri = 100$, $M_n = 0$ and $Pr = 6.93$.

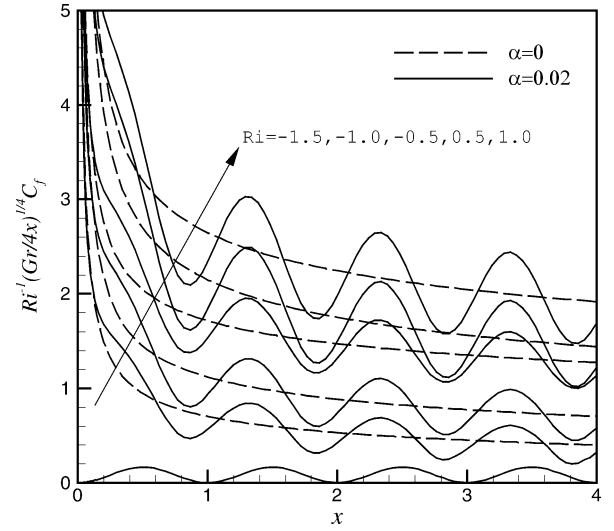

Fig. 14. Axial distribution of $Ri^{-1}(Gr/4x)^{1/4}C_f$ for different Richardson numbers at $\alpha = 0.02$, $Re = 1000$, $\phi = 30°$, $M_n = 1$ and $Pr = 6.93$.

the free convection becomes the dominant mode the skin-friction coefficient and the Nusselt number decrease as imposed on a magnetic field.

(c) The influence of the buoyancy parameter ($Ri/Re^{1/2}$ and Ri)

The axial distributions of $Ri^{-1}(Gr/4x)^{1/4}C_f$ and $(4/Gr_{\bar{x}})^{1/4}Nu_x$ are plotted in Figs. 12 and 13 with $\alpha = 0.1$, $Ri = 100$, $M_n = 0$ and $Pr = 6.93$. It is seen that the curves of $\phi = 30°$, $45°$ and $60°$ show a frequency equal to that of the wavy surface. The crests and troughs of $Ri^{-1}(Gr/4x)^{1/4}C_f$ and $(4/Gr_{\bar{x}})^{1/4}Nu_x$ occur near the crests and troughs of the wavy surface, where the inviscid free stream velocity is the maximum and minimum, which are shifted slightly upstream of the crests and troughs of the wavy surface by the buoyancy effect. Furthermore, an increase in the inclined angle tends to increase the values on the troughs for $Ri^{-1}(Gr/4x)^{1/4}C_f$ and $(4/Gr_{\bar{x}})^{1/4}Nu_x$. This indicated that the buoyancy force is seen to have a larger influence on the troughs of the wavy surface for different inclined angle. As seen more clearly in Figs. 12 and 13, for different buoyancy parameters $Ri/Re^{1/2}$, the quantities of $Ri^{-1}(Gr/4x)^{1/4}C_f$ and $(4/Gr_{\bar{x}})^{1/4}Nu_x$ have larger changes along the portion of the surface from crest to trough, where the slope S' and U'_w are negative. This result is due to the negative values decrease the effect of Ri but increase the effect of $Ri/Re^{1/2}$. However, for larger inclined angle (e.g., $\phi = 60°$), the influence of $Ri/Re^{1/2}$ becomes inconspicuous since the buoyancy parameter $Ri\sin\phi$ is much larger than another $Ri/Re^{1/2}\cos\phi$.

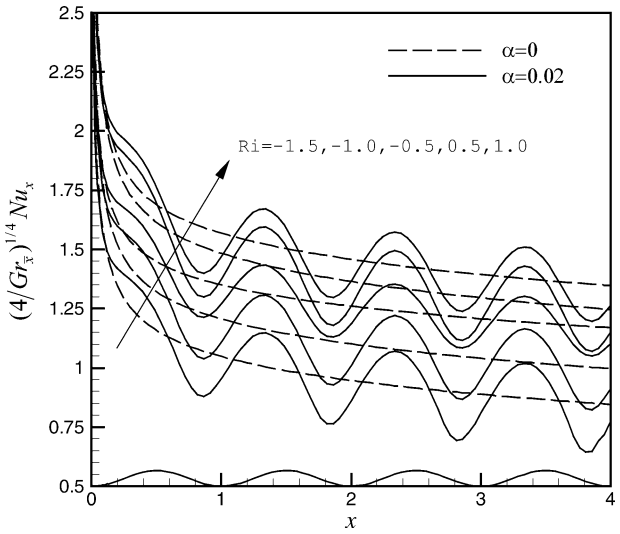

Fig. 15. Axial distribution of $(4/Gr_{\bar{x}})^{1/4}Nu_x$ for different Richardson numbers at $\alpha = 0.02$, $Re = 1000$, $\phi = 30°$, $M_n = 1$ and $Pr = 6.93$.

Figs. 14 and 15 also show variations of skin-friction coefficient and local Nusselt number along the wavy surface for different Richardson numbers. Clearly, for mixed convection, the skin-friction coefficient and the surface heat transfer rate will increase when the buoyancy force assists the forced flow (i.e., $Ri > 0$) and will decrease when it opposes the forced flow (i.e. $Ri < 0$). When the Richardson number decreases from 1 to -1.5, the amplitude of skin-friction coefficient tends to decrease. Moreover, comparing the wavy surface with the flat plate, the wavy surface has a smaller skin-friction coefficient in each furrow. This outcome predicts that the boundary layer will early separate (i.e., $C_f < 0$) from the furrows of wavy surface when the Richardson number decreases.

5. Conclusions

Mixed convection of boundary layer fluid along inclined wavy surfaces in the presence of a magnetic field has been analyzed by the Prandtl transformation method and the spline alternating-direction implicit method. Effects of the magnetic field parameter, the wavy geometry (i.e., the amplitude-wavelength ratio and the inclined angle), the buoyancy parameters (i.e., the Richardson number and the $Ri/Re^{1/2}$) and the Prandtl number on the skin-friction and on Nusselt number have been studied.

The effects of buoyancy increase with the Richardson number, the inclined angle and the amplitude-wavelength ratio, thereby causing increases in the average skin- friction coefficient and the average Nusselt number at the wavy wall. The larger buoyancy will make the skin-friction coefficient and the Nusselt number show the presence of the second harmonic for a wavy plate. Forced convection dominates the first harmonic at the smaller inclined angle or near the leading edge, while free convection dominates the second harmonic as the inclined angle increases or the fluid moves downstream. The influence of the buoyancy parameter $Ri/Re^{1/2}$ is obvious for the smaller inclined angle (e.g., horizontal wavy plate) and for the portion of the wavy surface from crest to trough. Moreover, the higher Prandtl number makes the skin-friction coefficient decrease and the Nusselt number increase. The magnetic field tends to increase the heat transfer rate when the buoyancy force is unapparent (e.g., smaller Richardson number; small inclined angle; near the leading edge of the plate). However, the heat transfer rate of the wavy plate is larger than that of the flat plate because of the larger heat transfer area. This fact may be helpful in choosing a proper heat transfer device for a given practical application.

References

[1] R.S.R. Gorla, Unsteady mixed convection in micropolar boundary layer flow on a vertical plate, Fluid Dynam. Res. 15 (1995) 237–250.
[2] T.Y. Wang, Mixed convection heat transfer from a vertical plate to non-Newtonian fluids, Internat. J. Heat Fluid Flow 16 (1995) 56–61.
[3] N. Ramachandram, B.F. Armaly, T.S. Chen, Mixed convection over a horizontal plate, ASME J. Heat Transfer 105 (1983) 420–423.
[4] F.S. Ibrahim, I.A. Hassanien, Mixed convection boundary layer flow of a micropolar fluid on a horizontal flat plate with power law variation in surface temperature, Internat. J. Thermal Sci. 39 (2000) 360–373.
[5] L.S. Yao, Natural convection along a vertical wavy surface, ASME J. Heat Transfer 105 (1983) 465–468.
[6] S.G. Moulic, L.S. Yao, Natural convection along a vertical wavy surface with uniform heat flux, ASME J. Heat Transfer 111 (1989) 1106–1108.
[7] D.A.S. Rees, I. Pop, A note on free convection along a vertical wavy surface in a porous medium, ASME J. Heat Transfer 116 (1994) 505–508.
[8] I. Pop, T.Y. Na, Natural convection of a Darcian fluid about a wavy cone, Internat. Com. Heat Mass Transfer 21 (1994) 891–899.
[9] C.P. Chiu, H.M. Chou, Transient analysis of natural convection in along a vertical wavy surface in micropolar fluid, Internat. J. Engrg. Sci. 32 (1994) 19–33.
[10] E. Kim, Natural convection along a wavy vertical plate to non-Newtonian fluids, Internat. J. Heat Mass Transfer 40 (1997) 3069–3078.
[11] S.G. Moulic, L.S. Yao, Mixed convection along a vertical wavy surface, ASME J. Heat Transfer 111 (1989) 974–978.
[12] I. Pop, S. Nakamura, Laminar boundary layer flow of power-law fluids over wavy surfaces, Acta Mech. 115 (1996) 55–65.
[13] F.S. Ibrahim, J.F. Hady, MHD mixed convection flow over a horizontal plate, Astrophys. Space Sci. 114 (1985) 335–344.
[14] A.A. Mohammadein, R.S.R. Gorla, Effects of transverse magnetic field on mixed convection in a micropolar fluid on a horizontal plate with vectored mass transfer, Acta Mech. 118 (1996) 1–12.
[15] L.S. Yao, A note on Prandtl's transposition theorem, ASME J. Heat Transfer 110 (1988) 503–507.
[16] C.Y. Cheng, C.C. Wang, Forced convection in micropolar fluid flow over a wavy surface, Numer. Heat Transfer Part A 37 (2000) 271–287.
[17] S.G. Rubin, R.A. Graves, Viscous flow solution with a cubic spline approximation, Comput. Fluids 1 (1975) 1–36.
[18] P. Wang, R. Kahawita, Numerical integration of partial differential equations using cubic spline, Internat. J. Comput. Math. 13 (1983) 271–286.